Journal of Nuclear Materials 399 (2010) 200–207

Contents lists available at ScienceDirect

Journal of Nuclear Materials

journal homepage: www.elsevier.com/locate/jnucmat

Effects of fast neutron irradiation on zirconium carbide

Lance L. Snead [a,*], Yutai Katoh [a], Sosuke Kondo [a,b]

[a] Materials Science and Technology Division, Oak Ridge National Laboratory, Oak Ridge, TN 37831, United States
[b] Institute for Advanced Energy, Uji Campus, Kyoto University, Japan

ARTICLE INFO

Article history:
Received 16 October 2009
Accepted 26 January 2010

ABSTRACT

High-purity zone refined zirconium carbide has been fast neutron irradiated in the dose and temperature range of 1–10 × 10^{25} N/m^2 (E > 0.1 MeV) and 635–1480 °C, respectively. Non-irradiated and as-irradiated properties were measured including the lattice parameter, hardness and elastic modulus as determined through nano-indentation, thermal conductivity, and indentation fracture toughness. The effects of neutron irradiation on the microstructure were also determined though using transmission electron microscopy. The general finding of this paper, limited to this particular zone refined ZrC of nominal C/Zr ratio of 0.93, is that this ceramic is quite stable under neutron irradiation in the temperature and dose range studied. Measurement of lattice parameter before and after irradiation indicated a lack of significant crystalline strain due to irradiation. Only modest changes were observed in the mechanical properties of hardness, elastic modulus, and indentation fracture toughness. The thermal conductivity underwent a slight reduction near 1000 °C irradiation, though was essentially unchanged for 1300–1480 °C irradiation. Transmission electron microscopy revealed black-spot-type defects (likely Frank or other small loops) for irradiation at 670 °C, maturing to faulted Frank loops at 1280 °C. As the irradiation temperature increased from 1280 °C to the highest irradiation temperature, of 1496 °C, a transition to prismatic loops occurs.

1. Introduction and background

Zirconium carbide is a candidate for use in high temperature gas cooled reactor fuels in three possible applications. First, microscopic ZrC powder may be used as an addition to the uranium oxide kernel of TRISO fuels to serve as an oxygen getter. Its presence is thought to buffer evolving oxygen liberated through the fission of UO_2 thereby avoiding adverse oxidative reactions, especially problematic at high fuel burn-up levels. The second application is the substitution of ZrC for SiC as the pressure vessel in TRISO fuel. The primary motivation for this substitution is the perceived enhanced high temperature properties of ZrC and its improved resistance to fission product attack and diffusion. This particular application has been investigated for decades, with fuels first produced and tested by Reynolds et al. [1] and more recent development carried out in Japan [2] and to a lesser extent in the US [3]. The third configuration combines both functions. Specifically, the fuel kernels would be coated directly with ZrC as an oxygen getter, or could be applied in addition to the SiC TRISO shell to enhance the performance of the fuel.

Since the initial work by Reynolds [1] there has been moderate investment in the development and irradiation of ZrC coated fuels (i.e. the second configuration above) with generally positive results. Specifically, these fuels have indicated probable higher temperature capability than SiC coated TRISO fuels [4–6] and enhanced resistance to the palladium fission product attack and diffusion that compromises SiC coated fuels [7,8].

While some of the researchers developing ZrC coated fuels have carried out reactor irradiation of their fuels, yielding essentially positive results, the irradiation effects on ZrC itself is still poorly understood. This is especially true if one limits the discussion to material types, irradiation conditions, and damaging doses relevant to ZrC fuel application. A review of the historic data is provided in the Appendix and summarized in Fig. 1. In this figure the existing irradiation effects literature data for all forms of ZrC are plotted as a function of irradiation temperature and dose. Inset to the figure are the operating temperature and dose regimes (approximate) for currently envisioned PBMR and GT-MHT fuels. Also included are the projected extended dose regimes for so-called Deep Burn fuels.

From Fig. 1 it is clear that the majority of the available literature data on ZrC irradiation effects is for lower temperatures, in most cases substantially lower, than the operating temperature regimes anticipated for TRISO fuel application. At the lower end of the inset operating temperature range for PBMR-type fuels are three studies either utilizing energetic protons [9,10] or krypton ions [11]. In each of these studies, hot-pressed ZrC was tested in the supersaturated carbon condition, $ZrC_{1.01}$. The quoted material density was reasonably high at 6.58 g/cm^3, which is ~99.5% of the theoretical

* Corresponding author. Tel.: +1 865 574 9942.
E-mail address: sneadll@ornl.gov (L.L. Snead).

0022-3115/$ - see front matter © 2010 Elsevier B.V. All rights reserved.
doi:10.1016/j.jnucmat.2010.01.020

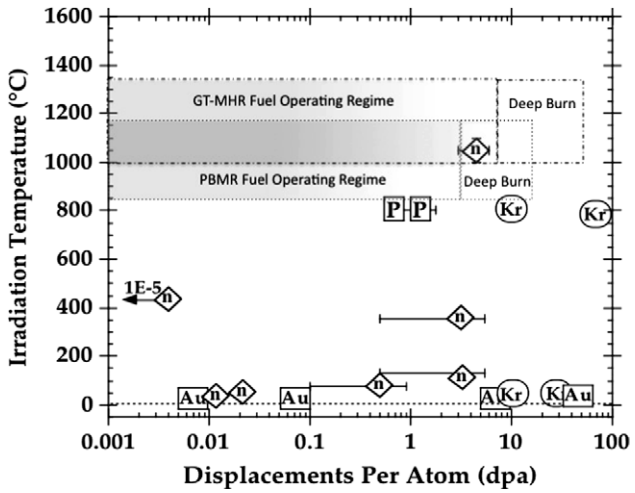

Fig. 1. Historic irradiation effects data on ZrC data compared to operating fuel temperature. DPA range data represented by bars, where appropriate. n: neutrons, Kr: krypton ions, Au: gold ions, P: protons [13,14,9–12,15–17].

density of stoichiometric material. Within the projected reactor temperature range of Fig. 1 there is only a single study (by Keilholtz), and that employed neutrons [12]. As noted in the Appendix the work of Keilholtz [12] reported on three types of powder processed ZrC materials in strongly carbon-rich condition (C/Zr ranging from 1.08 to 1.27) and quite low density (ranging from 70% to 95% theoretical).

This paper presents the effects of neutron irradiation on the microstructure and physical properties of a very high purity zirconium carbide in the temperature and dose range appropriate for high or very high temperature gas cooled reactor fuel application.

2. ZrC materials and experimental methods

Zirconium carbide is an extremely high-melting temperature carbide capable of existing over a wide range of carbon vacancy concentration while retaining a cubic NaCl-type crystal structure, the gamma phase. However, for C/Zr ratios exceeding unity the resulting structure is crystalline gamma phase ZrC with free carbon or graphite. The phase diagram for this system is given in Fig. 2. It is critically important that when discussing the properties of ZrC, whether non-irradiated or irradiated, the properties be put in the context of material stoichiometry. The reason for this is the significant effects of stoichiometry on physical properties. For example, within the range of the carbon deficient gamma phase (cf. Fig. 2) the density has been shown to vary by approximately 12%, hardness by approximately 40%, and thermal conductivity by approximately 600% [18]. Similar consideration must be given to the process by which the material is formed as this has a direct impact on purity and porosity (a contributor to density). For example, some studies of zirconium carbide [12,14,16] (see Appendix) utilized sintering aids (significant metallic additions) in the material processing, resulting in residual metal at grain boundaries and potentially within the crystal. As noted by inspection of the Appendix, theoretical density of materials studied to date has varied widely, from ~70% to ~99.5% dense.

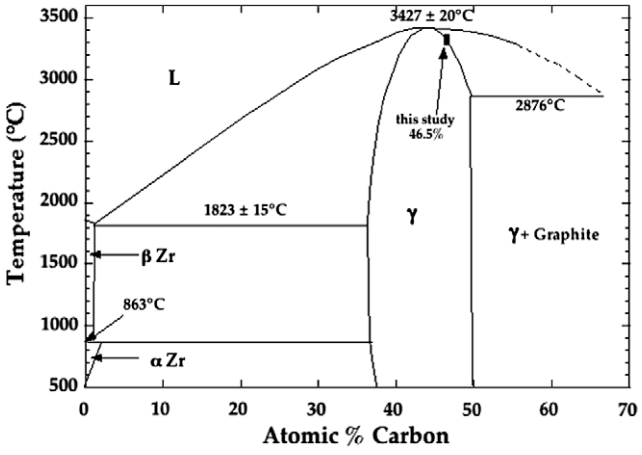

Fig. 2. ZrC phase diagram. Redrawn from [23].

All of the materials represented in the literature survey of Fig. 1 are powder process derived materials (see the Appendix) which is in contrast to the gas-phase decomposition chemical vapor deposition (CVD) process by which ZrC has been applied in TRISO fuel [1,19]. In contrast to powder processed materials, high quality CVD materials tend to have much less porosity and can in fact closely approach theoretical density. Moreover, CVD materials usually have much higher purity and relatively impurity-free grain boundaries. The stoichiometry of such material can be varied depending on processing and process variables, and as-deposited CVD [19–21] tends to range on the carbon-rich side of stoichiometry with C/Zr between 1.0 and 1.3. However, the current target stoichiometry in fuel development programs is 1.0. While this is subject to change as better information becomes available, the data suggests that straying from stoichiometry on the side that induces free carbon and graphite formation promotes enhanced metallic fission product diffusion, [21] while moving away from stoichiometry on the side of structural carbon vacancies promotes the diffusion of gaseous fission products [22].

This work determines the fundamental neutron irradiation performance for zirconium carbide at relevant environments for gas reactors with a material relevant to the application. Sample sizes of CVD ZrC appropriate for thermophysical property measurement are not yet available. Zone refined material, as a near fully dense, pure material of tailored stoichiometry was therefore chosen, with stoichiometry between that resulting in the maximum melting temperature and purely stoichiometric material. Specifically, 46.5 atomic percent carbon ZrC, thus C/Zr of 0.87, was selected, which is somewhat higher than the 43.8% needed to give the maximum melting temperature in the phase diagram (Fig. 2) [23]. The material was produced by Applied Physics Technology, Inc., of McMinnville Oregon.

The zone refined rods of approximately 6 mm diameter were large grained ZrC of >98% theoretical density. Spark discharge impurity analysis by Shiva Technologies showed that most metallic impurities were either lower than detection limits or at levels less that 10 wt. parts per million. Elements in excess of this value included Na (100 wppm), Si (15), K (69), and Hf (30). Fig. 3 shows polished metallographic sections. The left image of Fig. 3 shows a relatively low magnification end-on view of the rod demonstrating the large grains (up to ~100 μm) formed during solidification. The right image is a section of the same material taken along the cylinder axis clearly showing grain elongation along the direction of solidification.

Specimens were irradiated in the Flux Trap of the High Flux Isotope Reactor (HFIR) at nominal fast and thermal neutron fluxes of 9×10^{18} N/m^2 s ($E > 0.1$ MeV) and 2.5×10^{19} N/m^2 s, respectively. Two types of irradiation vehicles were used. The METS series were three fixed capsules irradiated in HFIR with irradiation temperatures ranging from ~970 °C to 1496 °C. The fluence ranged from 0.8 to 9.38×10^{25} N/m^2 ($E > 0.1$ MeV). The irregular (nominal 6 mm diameter) ZrC cylinders were loaded in holders within the METS capsule with each sample at a different irradiation temperature. The samples were in high-purity graphite holders in a sealed

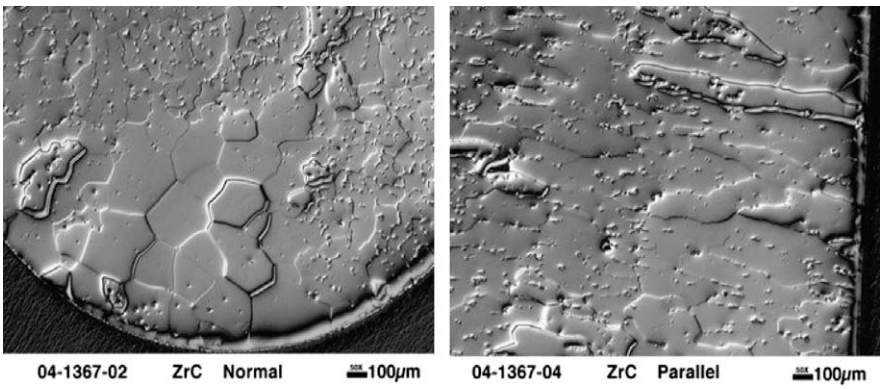

Fig. 3. Metallographic section of zone refined ZrC. Left: axial view of rod. Right: cylindrical direction view of rod.

high purity argon environment. Both fixtures on the ends of the holders were threaded graphite caps that included eight cylindrical wells, each containing a melt wire. The melt wires were pure materials or binary alloys blended to achieve a specified melting temperature. For each position in a capsule the design temperature was achieved by varying the gas gap between the outside of the sample holder and the inner wall of the capsule. The maximum temperature of the holder during irradiation was determined by inspecting the melt wires following irradiation. The melt wires were selected to allow for either an overestimation or underestimation of the actual temperature of the holder. Melt wires were chosen in ~20–40 °C increments around the design temperature. A temporal variation in temperature within a holder was expected due to the radiation-induced dimensional change of the Poco AXF-5Q graphite holder (thus changing the gap between the sample holder and capsule containment). No change in temperature due to variation in reactor power was expected due to the exceptionally steady power history of the HFIR reactor during the irradiations. The error bars associated with the temperature data shown for the METS samples are a combination of the melt wire observation and calculated variation based on the expected changing gas gap.

A second type of irradiation capsules (rabbit capsules) were used in the HFIR experiments. Small bars and transmission electron microscopy (TEM) samples were inserted into graphite holders, placed in aluminum outer capsule and seal welded under ultra high purity argon. The sample irradiation temperatures were achieved by varying the gap thickness between the holder and the inner wall of the aluminum rabbit capsule. The irradiation temperature of the rabbit capsules was measured by post-irradiation isochronal annealing of SiC temperature monitors using the electrical resistivity technique [24]. The temperature for this series of irradiations ranged from ~635 °C to 1080 °C with neutron doses ranging from 1.92 to 4.24 × 10^{25} N/m^2 (E > 0.1 MeV).

Samples were prepared for indentation mechanical property measurements by diamond lapping to a final finish of 0.5 microns. In all cases a significant depth of surface material was removed prior to achieving a final mirror-like polish. The effect of load on measured hardness was evaluated over a wide range with little observed effect, so an applied load of 1.96 N was chosen for the reported data. TEM samples were prepared by standard cutting, grinding, and ion-milling techniques. X-ray diffraction patterns were collected using a PANalytical θ–θ diffractometer with Cu Kα radiation, variable slits to enhance the intensity back reflection region and solid state line detector. The intensity data were converted to equivalent fixed slit geometry values for analyses.

Specimens from METS rod irradiations were cut to 5.8 mm diameter with nominally 0.5 or 2.5 mm thickness; rabbit capsule specimens were cut to thin strips. Both types were mechanically polished to <~15 μm thickness. Thin foils were prepared in a commercial Ar-ion-milling unit (FISCHIONE model 1010) using a 3–5 keV very low angle beam. Microstructures were studied using a conventional TEM (Philips/FEI Technai 20, 200 keV).

3. Results and discussion

3.1. Microstructural evolution

As outlined in the Appendix, a number of researchers have reported the effects of ion irradiation on the microstructure of hot-pressed zirconium carbide. For implantation near room temperature [11,15] the observed result was the typical black dot microstructure and dislocation networks. Given the extremely high-melting temperature of the $ZrC_{1.01}$ (somewhat lower than 3149 K), room temperature is <0.1 of the homologous temperature and such a high density of very small and practically unresolvable defects is expected. For the microstructural observations following proton or Kr irradiations near 800 °C, the researchers identified nanometer size Frank loops (~1.5 dpa) and small faulted loops [9]. Also, Gan [11] observed "precipitation-type" formation as a result of his room temperature and 800 °C Kr irradiation for the dose range 10–70 dpa.

TEM imaging of the non-irradiated material used in this study reveals a material essentially free of defects and voids. Representative results from the microstructural examination of the neutron irradiated ZrC are given in Fig. 4. At the low and intermediate temperature (~660–1023 °C) TEM reveals similar microstructures where the dominant defects are unidentified loops, some of which are aligned in raft structures (Fig. 4, left). However, in comparison to the 660 °C microstructure, additional loops of somewhat larger size are identified as Frank loops formed on {1 1 1} during the 1023 °C irradiation. As the irradiation temperature increased from ~1023 °C to 1260 °C the microstructure of ZrC evolved to a mixed population of distinct Frank loops and loops with Burgers vector not corresponding to the Frank loop, b = 1/3 ⟨1 1 1⟩. For the highest temperature irradiation (~1496 °C), the microstructure further evolved into prismatic loops. Small voids, on the order of 5 nm, were found in the highest dose, high irradiation temperature sample (5.8 × 10^{25} N/m^2, 1496 °C), but the number density of these voids was extremely low.

An analysis of the microstructural evolution in terms of the measured loop diameter and number density is provided in Figs. 5 and 6. Fig. 5 shows a clear trend towards loop growth with temperature. Noting that the data presented represent a range in fluence, shown numerically above the symbols in the figure, it is also clear that the loop diameter tends towards growth with increasing fluence. As the temperature was increased there was also a clear trend towards reduced loop density, as indicated in Fig. 6. The

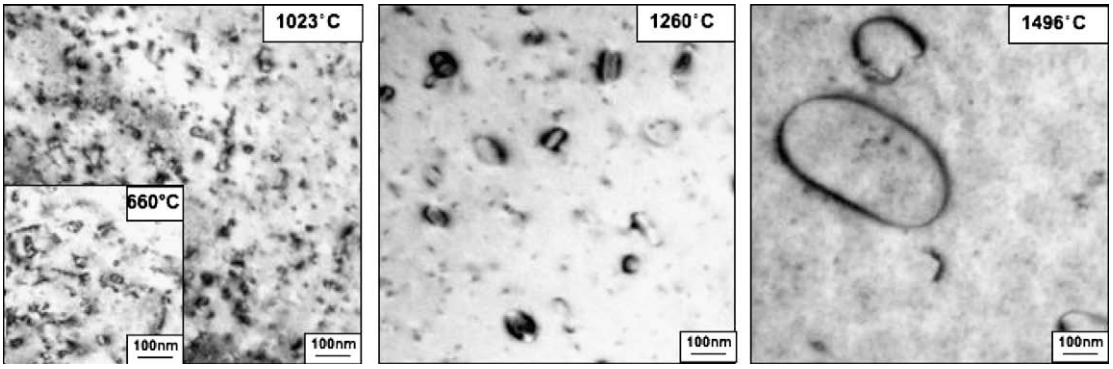

Fig. 4. Left-unidentified small loops at dose level of 3.7×10^{25} N/m^2, 660 °C and 2.0×10^{25} N/m^2, 1023 °C. Middle-mixed Frank and (most likely) prismatic loops for 9.4×10^{25} N/m^2, 1260 °C. Right-large prismatic loop at 5.8×10^{25} N/m^2, 1496 °C.

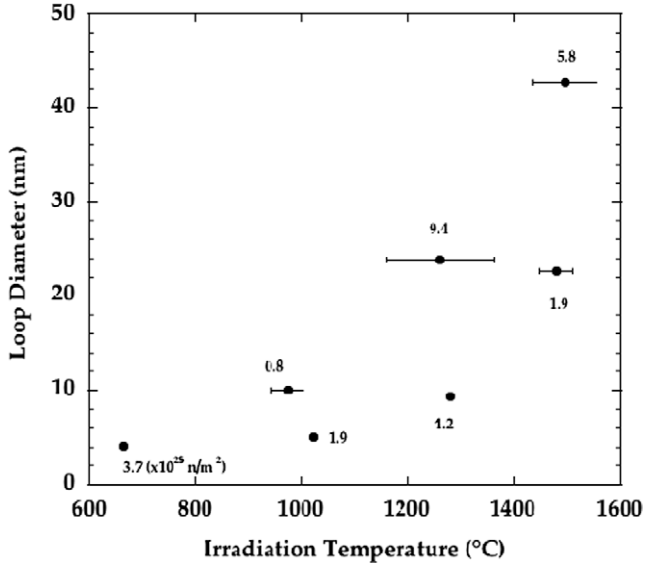

Fig. 5. Measured loop diameter in neutron irradiated ZrC as a function of irradiation temperature. Inset numbers refer to fast neutron fluence.

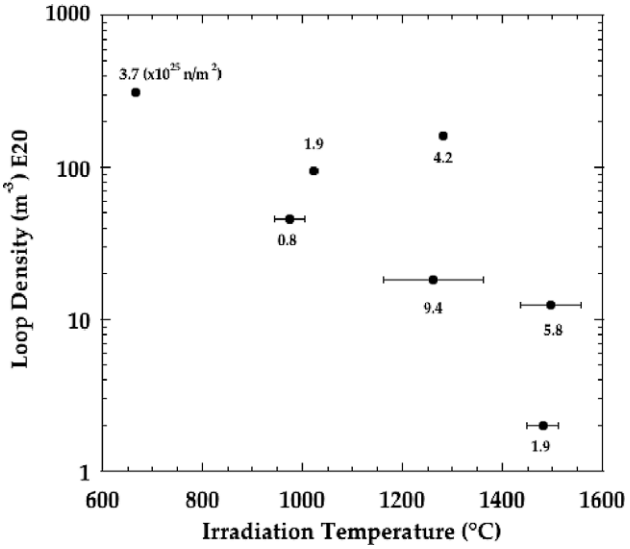

Fig. 6. Measured loop density in neutron irradiated ZrC as a function of temperature. Inset numbers refer to fast neutron fluence.

relationship between loop density, loop size, and irradiation temperature is perhaps more clearly seen in Fig. 7, which gives the distribution of loop sizes as a function of irradiation temperature. It is noted that Figs. 5–7 combine Frank and prismatic loops, and as seen in Fig. 4 there is a transition from the intermediate temperature Frank loops to higher temperature prismatic loop formation. The relative distribution of Frank and prismatic loops at the "transition" temperature of 1260 °C is shown in Fig. 8.

3.2. Swelling

The swelling of neutron irradiated ZrC whether determined from crystal strain (X-ray) or through geometric swelling measurement, has been reported by several researchers with somewhat inconsistent results [10–14,16,25].

With the exception of Gan [11], who reported an unexpected and unexplained 7% lattice expansion for his 70 dpa, 800 °C Kr irradiation, crystal lattice expansion due to irradiation is <1%. Near

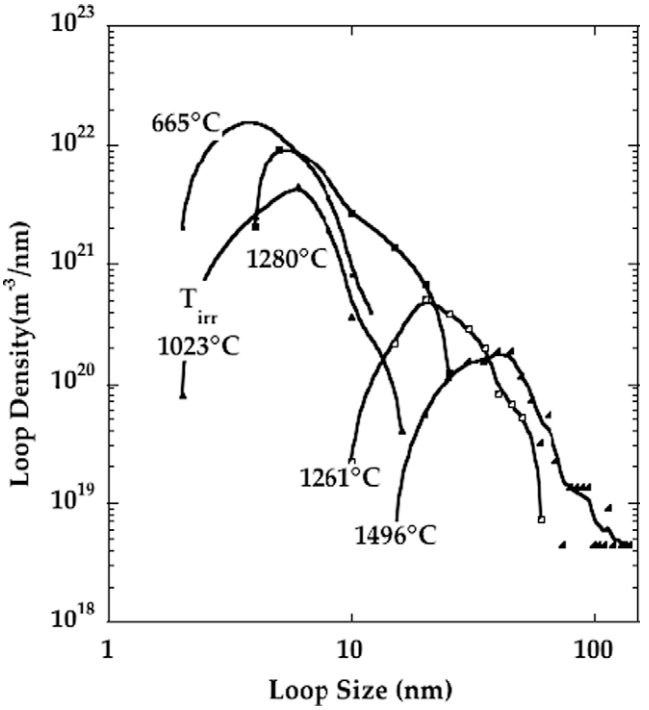

Fig. 7. Loop size distribution in irradiated ZrC as a function of irradiation temperature. Loop density axis gives the as number density per nm-wide element of loop size (bin width). Temperature indicated are mean irradiation temperatures.

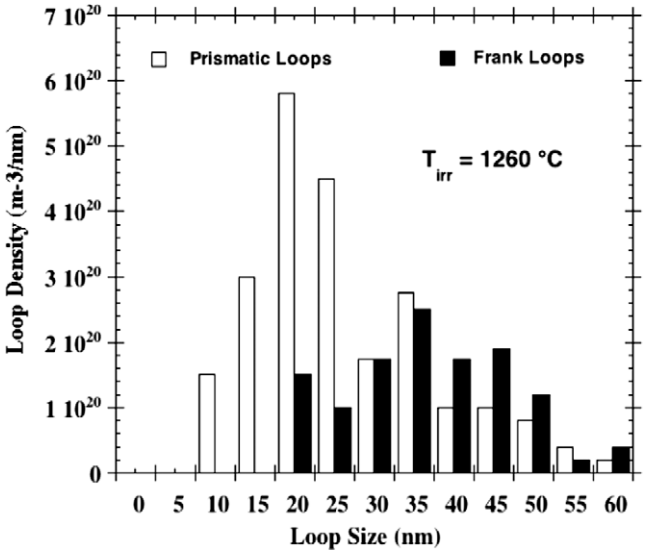

Fig. 8. Differentiation between Prismatic and Frank Loops for ZrC irradiated at ~1260 °C.

room temperature, the gold ion irradiation of Gossett [15] showed a saturation of 0.1% lattice parameter increase by 0.1 dpa. For the proton irradiation at 800 °C of Yang [10] the swelling is seen to increase with irradiation and perhaps approach a saturated value somewhat above 0.11% by 1.5 dpa.

It is noted that the early work of Keilholtz [16] on carbon-rich ZrC (C/Zr: 1.08–1.27) reported gross volume swelling (dimensional changes) in the range of 2–2.7% for three types of powder processed ZrC, while the volume calculated from lattice expansion of the 130–355 °C neutron irradiated samples was ~0.2–0.8%. Keilholtz [12] goes onto report that their materials underwent "minor to severe fracturing" for doses greater than 1.6 dpa. It is most likely that the microcracking which led to the eventual fracturing also contributed to the reported gross volume change. For a higher dose neutron irradiation Keilholtz later reported [12] that no fracture occurred for identical materials at an irradiation temperature of 1000–1100 °C, with no significant change in lattice parameter. This work is suggestive of simple defect driven crystal strain, which would increase with decreased irradiation temperature, leading to eventual disruption of the ZrC grain boundaries.

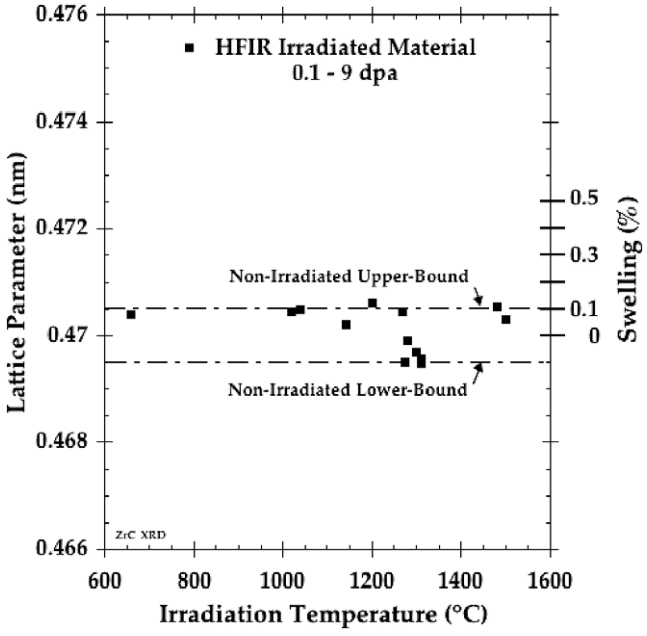

Fig. 9. Lattice parameter of irradiated ZrC compared to range of non-irradiated lattice parameter.

As briefly mentioned in the introduction, stoichiometry can have a large effect on the lattice parameter, hence density, of ZrC. While the material of the present work was within a fairly narrow range of C/Zr ratio, there was still a slight sample-to-sample variation in X-ray lattice parameter. The lattice parameter was determined over the entire range of neutron dose and irradiation temperature of this study and the data are presented in Fig. 9. The as-irradiated data are clearly seen to range between the upper and lower bounds of the non-irradiated lattice parameter. While there may have been some systematic change in lattice parameter due to irradiation, none can be detected within the scatter of the non-irradiated values. However, as shown by the right axis of the figure, any effect of neutron irradiation on the lattice parameter is necessarily <0.2%. This result is therefore in basic agreement with very modest lattice parameter changes noted by the majority of researchers. Moreover, measurement of physical dimensions did not support any gross volumetric change in excess of that calculated from the lattice parameter change. Through optical and scanning electron microscopy imaging of polished surfaces it was clear that, at the doses of this study (which were higher than those of Keilholtz) no disruption of grain boundaries or fracturing of samples occurred.

3.3. Micromechanical properties

Hardening of ZrC measured by micro-indentation has been reported previously. Kovalchenko carried out 50 °C neutron irradiation of hot-pressed $ZrC_{0.98}$ and reported a 12% increase in hardness for an approximate 0.02 dpa dose [25]. Yang reported a 10–15% increase for $ZrC_{1.01}$ proton irradiated at 800 °C to 1.5 dpa [10]. In the current work both micro-indentation hardness (1.96 N applied load) and nano-indentation (0.45 N maximum applied load) was measured. It is important to note that the hardness of ZrC is known to depend on the loading orientation with respect to the crystal orientation. Specifically, Hannink [26] has shown hardness for the indenter oriented 90° to the [1 0 0] direction to be ~19.4 GPa while it reaches a maximum of ~22.2 GPa at an orientation of 45° to [1 0 0]. As the grain size for the material of the current study is relatively large compared to the indents, individual measurements are expected to show some variation as they will be sampling random crystal orientations. Vickers micro-hardness values of non-irradiated and irradiated ZrC are presented in Fig. 10. Each data-point represents an average of more than ten indents +/− standard deviation. The intrinsic variability of the samples, and the effect of crystal orientation, is clearly evident in the scatter of the non-irradiated hardness (left of figure). These data do not show a strong effect of irradiation temperature on irradiation hardening, though a modest increase consistent with the previous work is plausible. Within the statistical scatter, the presence of hardening may be more convincingly evident by inspection of the inset in Fig. 10, which provides hardness as a function of irradiation dose combined for all irradiation temperatures. Again, an increase in hardness consistent with earlier findings (about 10–15%) is plausible.

The trend in hardness measured by nano-indentation agrees well with the Vickers hardness (Fig. 10), though the nano-hardness data is systematically slightly higher (on the order of a 3–5 GPa). The reason for this minor difference is not clear. However it is noted that the maximum load applied during nano-indentation was 0.45 N compared with the 1.96 N applied in the Vickers testing. While a systematic change in Vickers hardness was not

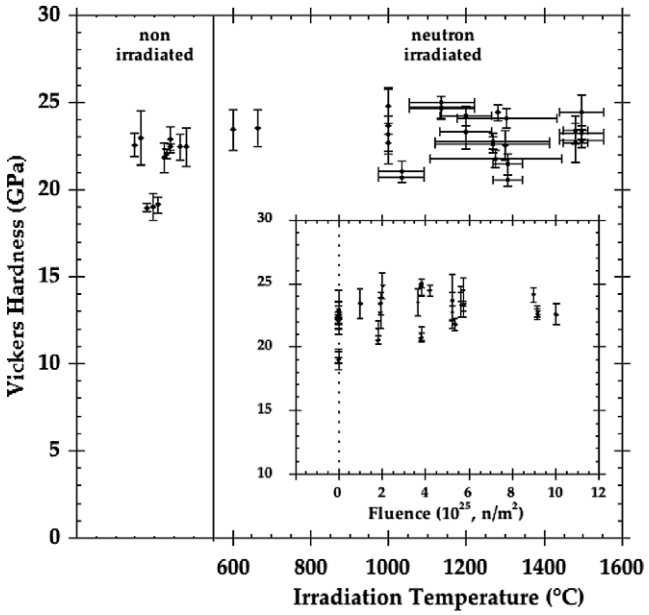

Fig. 10. Effect of neutron irradiation on Vickers hardness of ZrC.

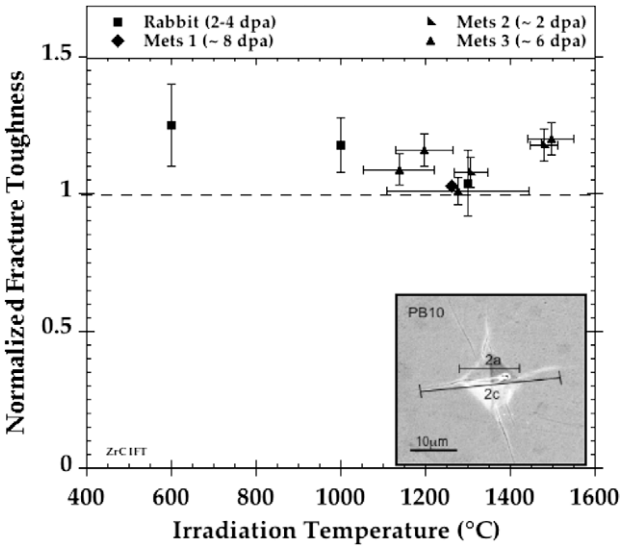

Fig. 12. Indentation fracture toughness of irradiated ZrC normalized to non-irradiated value.

observed over the range of load studied (0.98–2.29 N) it is possible that the materials response to a lower load would yield the slightly higher hardness measured with nano-indentation. Such a difference may also be consistent with the difference between manual determination of indent size during the Vickers process and the automated nano-hardness calculation, or may possibly be an effect of surface condition. Fig. 11 shows the elastic modulus obtained from the nano-indentation measurements. In this case a more clear increase due to irradiation is indicated.

The indentation fracture toughness of irradiated ZrC is presented in Fig. 12. A real increase in indentation fracture toughness with irradiation using the relationship of Ponton and Rawlings (K = constant $(P/L)^{1/2}$; where P is load, L length of crack $(c–a)/2$ in the figure inset) is shown [27]. There appears to be a reduction in the irradiation-induced toughening as irradiation temperature is increased, then an approach to the non-irradiated value. This transition corresponds roughly to the transition from the temperature regime where a high density of unidentified loops and "black dots" dominate to the regime where large Frank loops and prismatic loops dominate.

3.4. Thermal properties

As mentioned in Section 2, the thermal transport within ZrC is highly dependent on stoichiometry. In the structural vacancy regime (C/Zr < 1), the thermal conductivity of hot-pressed ZrC has a relatively constant value of 8–11 W/mK for C/Zr ratios in the range 0.6–0.9. As the C/Zr ratio approaches unity the thermal conductivity rapidly increases to nearly 45 W/mK [18]. The material for this study is in the upper end of that C/Zr ratio, ~0.87, and the measured, non-irradiated, room temperature thermal conductivity for this material is somewhat higher than the values for hot-pressed material. Specifically, values for the non-irradiated material ranged from 12 to 16 W/mK at room temperature. A particular feature of ZrC is that both electrons and phonons contribute significantly to conductivity near room temperature, and their contribution are

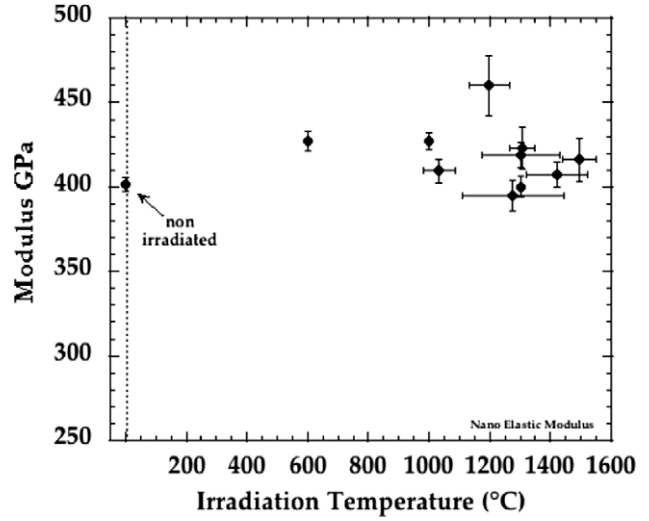

Fig. 11. Effect of neutron irradiation on elastic modulus as measured by nano-indentation.

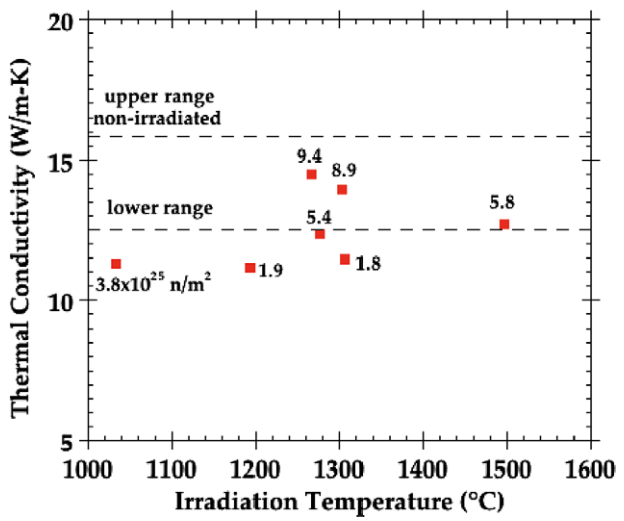

Fig. 13. Effect of neutron irradiation on thermal conductivity of ZrC. Inset numbers refers to fast neutron fluence.

additively: (i.e. $K_{total} = K_{electron} + K_{phonon}$). Moreover, the electrical conductivity increases with increasing temperature as does the total conductivity. For this zone refined ZrC, the Wiedeman–Franz law and the electrical conductivity give a calculated electronic contribution to conductivity of ~7 W/mK. The difference between this value and the measured thermal conductivity is then attributed to phonon transport.

The as-irradiated measured values of thermal diffusivity are given in Fig. 13. A minor degradation in thermal conductivity appears to have occurred, with this degradation more pronounced at the lower irradiation temperature. As the irradiation did not produce an appreciable change in electrical conductivity of the sample the degradation in thermal conductivity is attributed to phonon-scattering from irradiation-produced defects. This assumption is consistent with the apparent larger reduction in conductivity for the lower temperature irradiation.

The evolving microstructure, while not having near the catastrophic effect seen in early powder metallurgy derived forms of ZrC, did result in slight mechanical property changes. A modest increase in hardness and indentation fracture toughness was measured while a very minor decrease in elastic modulus and thermal conductivity was also observed. The swelling of ZrC over the temperature and dose ranges evaluated, if present, was <0.2%. There were no changes in grain boundaries of the materials revealed by TEM, SEM, or optical microscopy examination.

The overall finding of this work is that for the neutron dose and temperature range appropriate to the application of ZrC in TRISO fuel application, the ZrC, at least in the carbon deficient stoichiometry ratio of $ZrC_{0.87}$, is quite stable. Further work to investigate a wider range of stoichiometry and to eventually include chemical vapor deposited material is suggested.

4. Conclusions

This work is the first investigation of the effects of neutron irradiation on the microstructure of zirconium carbide. For the high-purity zone refined $ZrC_{0.87}$, irradiation near 660 °C produced a dense network of unidentified loops which were somewhat coarsened and identified as Frank loops after irradiation at 1023 °C. In the irradiation temperature range 1023–1260 °C the microstructure coarsened and the defects made a transition from predominantly Frank loops to prismatic loops. At the highest temperature studied, 1496 °C, the as-irradiated microstructure was dominated by large prismatic loops. At this highest irradiation temperature, while very small voids were identified, their size was very small and their concentration was extremely low.

Acknowledgements

The authors would like to thank Joel McDuffee and Bob Sitterson for their assistance with the irradiation experiments. Irradiations were carried out in the US Department of Energy (DOE) Basic Energy Science Sponsored High Flux Isotope Reactor. The authors would also like to thank Dr. Tom Watkins of the Thermophysical Properties User Center of the Oak Ridge National Laboratory for assistance with the X-ray characterization. Research was sponsored by the DOE Office of Nuclear Energy as part of an International Nuclear Energy Research Initiative project and the Deep Burn Project. Work was carried out at the Oak Ridge National Laboratory for US Department of Energy under Contract DE-AC05-00OR22725 with UT-Battelle, LLC.

Appendix A

References	Material	Temperature	Dose and species[d]	Property evolution
Gossett [15]	*Hot pressed* 85% dense	RT	4 MeV Au irradiation	0.15% swelling, saturated by 0.1 dpa Formation of small, faulted dislocation loops
			7–35 dpa (peak)	Dislocation network formed at high doses Formation of zirconium oxide phase noted
Gan [11]	*Hot pressed* C/Zr = 1.01	27 °C and 800 °C	1 MeV Kr 10–30 dpa at 27 °C	27 °C: black dot microstructure ~0.7–0.9% lattice parameter increase 800 °C: precipitate formation
	Density 6.58 g/cc (~99.5% theoretical)		10 and 70 at 800 °C	~0.6–7.0% lattice parameter increase
Gan [9]	*Hot pressed* C/Zr = 1.01 Density 6.58 g/cc (~99.5% theoretical)	800 °C	2.6 MeV proton 0.71–1.8 dpa	Formation of small faulted loops
Taubin [28]	Zr–C0.96	<430 °C	Mixed fission neutrons $\sim10^{-5}$ dpa	In-situ property measurement Minor changes in thermal conductivity, thermal expansion, heat capacity, and electrical resistivity
Andrievskii [13]	Unknown C/Zr range (0.7–0.93)	140 °C	Neutrons ~0.01 dpa	~0.35% lattice expansion for C/Zr of 0.93
Yang [10]	*Hot pressed* C/Zr 1.01 Density 6.58 g/cc (~99.5% theoretical)	800 °C	2.6 MeV proton 0.7–1.5 dpa	*Frank loops observed* ~0.11% lattice parameter increase ~10–15% increase hardness Significant increase in indent fracture toughness
Kovalchenko [25]	*Hot pressed* ZrC0.98 Porosity <4%	~50 °C	Neutrons <0.02 dpa	Up to 0.321% lattice expansion Up to 12% increase in hardness

Appendix A (*continued*)

References	Material	Temperature	Dose and species[d]	Property evolution
Keilholtz [16]	*Hot pressed*	130–355 °C[a,b]	Neutrons	*Hot pressed*
			~1.8–6.6 dpa	Volume change from lattice expansion ~0.2–0.8%
	6.3 g/cc,93% theoretical		~1.6–3.4 dpa	Gross volume expansion 2.3–2.7%
	C/Zr 1.08			Minor to severe fracturing above 1.6 dpa
	1 wt.% impurities		~1–3.5 dpa	*Slip cast*
	Slip cast			Gross volume expansion 2–2.5%
	4.7 g/cc, 70% theoretical			Minor to severe fracturing above 1.6 dpa
	C/Zr 1.20			*Explosion bonded*
				Volume change from lattice expansion ~0.6%
	1.5 wt.% impurities			Gross volume expansion 2.1–2.6%
	Explosion bonded[c]			Minor to severe fracturing above 1.6 dpa
	6.4 g/cc, 95% theoretical			
	C/Zr 1.27			
	0.55 wt.% impurities			
Keilholz [12]	*Hot pressed*	1000–1100 °C[a]	Neutrons	*Hot pressed*
			~5.9 dpa	Gross volume expansion 0.1%
				No fracture observed
				Slip cast
	6.3 g/cc, 93% theoretical		~2.9–6 dpa	Gross volume expansion 0.9–0.7%
				No fracture observed
	C/Zr 1.08			*Explosion bonded*
	1 wt.% impurities			Gross volume expansion 1%
	Slip cast		~3 dpa	No fracture observed
	4.7 g/cc, 70% theoretical			
	C/Zr 1.20			
	1.5 wt.% impurities			
	Explosion bonded[c]			
	6.4 g/cc, 95% theoretical			
	C/Zr 1.27			
	0.55 wt.% impurities			
Dyslin [14]	Hot pressed	65–90 °C[a]	~0.15–0.9 dpa	Volume expansion 0.017–0.021%
	Slip cast			No dependence on materials exhibited
	Explosion bonded (see Keilholtz description)			

[a] Reported as calculated temperatures. True temperatures may be significantly different.
[b] Irradiation temperature reported as 300–700 °C in original reference. However, calculated irradiation temperature was revised as reported by Dyslin [12].
[c] Few percent Ni or Co added to powder prior to explosive bonding. Resulting material includes ~5% residual Ni/Co at grain boundaries.
[d] The displacement damage listed is as provided in original reference for ion irradiation. For neutron irradiation an equivalency of 1 dpa = 1×10^{25} N/m^2 ($E > 0.1$ MeV) or 0.8×10^{25} N/m^2 ($E > 1$ MeV) is assumed. It is noted that such an equivalency is appropriate for lower Z carbides [29] but is likely an over estimate of dpa for ZrC.

References

[1] G.H. Reynolds et al., J. Nucl. Mater. 62 (1976) 9.
[2] S. Ueta et al., J. Nucl. Mater. 376 (2008) 146.
[3] R.M. Versluis et al., HTR2008 85325 (2008).
[4] T. Ogawa et al., Research and development of ZrC-coated UO_2 particle fuel at JAERI, in: Conference on Nuclear Fuel Performance, Published by British Nuclear Energy Society, London, 1985.
[5] T. Ogawa et al., J. Am. Ceram. Soc. 75 (1992) 2985.
[6] T. Ogawa, K. Ikawa, J. Nucl. Mater. 99 (1982) 85.
[7] T. Ogawa, K. Ikawa, J. Nucl. Mater. 22 (1986) 179.
[8] T. Ogawa, K. Fukuda, ZrC Coated Particle Fuel Development, JAERI-M 92-207 (1992), pp. 554.
[9] J. Gan, Y. Yang, C. Dickson, T. Allen, J. Nucl. Mater. 389 (2009) 317.
[10] Y. Yang et al., J. Nucl. Mater. 378 (2008) 341.
[11] J. Gan, M.K. Meyer, R. Birtcher, T.R. Allen, J. ASTM Int., JAI12376 3 (2006) 1.
[12] G.W. Keilholtz, R.E. Moore, D.A. Dyslin, Fuels Mater. Develop. Quart. Prog. Rept., ORNL-4390 (1968) 113.
[13] R.A. Andrievskii, V.I. Savin, V.V. Ya Markin, V.T. Spravtsev, A.S. Shevcenko, Neorg. Mater. 14 (1978) 526.
[14] D.A. Dyslin, R.E. Moore, H.E. Robertson, ORNL-4480 (1969) 245.
[15] D. Gosset, M. Dolle, D. Simeone, G. Baldinozzi, L. Thorne, J. Nucl. Mater. 373 (2008) 123.
[16] G.W. Keilholtz, R.E. Moore, M.F. Osborne, Nucl. Appl. 4 (1968) 330.
[17] M.S. Kovalchenko, Y.I. Rogoval, Neorg. Mater. 9 (2) (1973) 321.
[18] E.K. Storms, P. Wagner, High Temp. Sci. 5 (1973) 454.
[19] T. Ogawa, K. Ikawa, K. Iwamoto, J. Nucl. Mater. 97 (1981) 104.
[20] K. Minato, T. Ogawa, K. Fukuda, Review of Experimental Studies of Zirconium Carbide Coated Fuel Particles for High Temperature Gas Cooled Reactors, JAERI-Review 95-004, 1995.
[21] K. Fukuda, K. Ikawa, K. Iwamoto, J. Nucl. Mater. 87 (1979) 367.
[22] A. Auskern, J. Nucl. Mater. 22 (1967) 257.
[23] T.B. Massalski, Binary Alloy Phase Diagrams, second ed., Materials Information Society, 1996. vol. 1.
[24] L.L. Snead, A.M. Williams, A.L. Qualls, Revisiting the use of SiC as a post irradiation temperature monitor, in: The Effects of Radiation on Materials: 21st International Symposium, 2003.
[25] M.S. Kovalchenko, Y.I. Rogavoi, Neorganicheskie Materlaly 9 (1973) 321.
[26] R.H.J. Hannink, D.L. Kohlstedt, M.J. Murray, Proc. Roy. Soc., Lond. A32 (1972) 409.
[27] C.B. Ponton, R.D. Rawlings, Mater. Sci. Technol. 5 (1989) 865–872.
[28] M.L. Taubin, S.V. Fateev, M.V. Ivanov, P.V. Shutov, At. Energy. 70 (1991) 55.
[29] S.J. Zinkle, C. Kinoshita, J. Nucl. Mater. 251 (1997) 200.